



Laser Patterning Pretreatment before Thermal Spraying: A Technique to Adapt and Control the Surface Topography to Thermomechanical Loading and Materials

Robin Kromer, Sophie Costil, Jonathan Cormier, Laurent Berthe, Patrice Peyre, and Damien Courapied

(Submitted May 7, 2015; in revised form October 3, 2015)

Coating characteristics are highly dependent on substrate preparation and spray parameters. Hence, the surface must be adapted mechanically and physicochemically to favor coating–substrate adhesion. Conventional surface preparation methods such as grit blasting are limited by surface embrittlement and produce large plastic deformations throughout the surface, resulting in compressive stress and potential cracks. Among all such methods, laser patterning is suitable to prepare the surface of sensitive materials. No embedded grit particles can be observed, and high-quality coatings are obtained. Finally, laser surface patterning adapts the impacted surface, creating large anchoring area. Optimized surface topographies can then be elaborated according to the material as well as the application. The objective of this study is to compare the adhesive bond strength between two surface preparation methods, namely grit blasting and laser surface patterning, for two material couples used in aerospace applications: 2017 aluminum alloy and AISI 304L stainless steel coated with NiAl and YSZ, respectively. Laser patterning significantly increases adherence values for similar contact area due to mixed-mode (cohesive and adhesive) failure. The coating is locked in the pattern.

Keywords adhesion testing, thermal barrier coating, atmospheric plasma spray (APS), Nd-YAG laser, laser surface texturing, grit-blasting

1. Introduction

New processes and materials are emerging with specific properties or endurance life and/or lower environmental impact. In this approach, surface treatments carried out by thermal spraying appear quite promising, as they can extend the life of components while improving their performance (Ref 1). The adhesion of thermally sprayed coatings strongly depends on the substrate topography (wettability, contact area) (Ref 2), substrate temperature (coating/substrate gradient temperature) (Ref 3), and surface composition (physicochemical contact) (Ref 4). Surface cleanliness is a key parameter for coating quality

(Ref 5). Both substrate and coating temperature also control the residual stress distribution (Ref 6).

Adhesion is related to the nature and strength of the bonding forces between two materials, such as ionic, covalent, metallic, hydrogen, and van der Waals forces (Ref 7). Practical adhesion adds mechanical anchoring effects. Generally, oxides, carbon, and oils have to be removed from the surface (particularly for metallic surfaces) before final use, as they change the physicochemical characteristics and/or contact surface (Ref 8). Among other methods, degreasing and grit blasting are classical procedures applied prior to thermal spraying. Degreasing involves chemical modification of the surface, while grit blasting modifies the surface morphology by creating a uniform roughness that provides mechanical interlocking of the particles to the substrate (Ref 9). Grit-blasted surfaces are contaminant free with abrasive granules. This technique is very effective for most materials, but ductile materials may be damaged with severe surface plastic deformation and/or microcracks (Ref 10). In addition, grit inclusion can occur, decreasing the adherence of the subsequent coating. New technologies such as laser tools have been developed to adjust the coating–substrate adhesion, but they also suffer from some disadvantages. Laser tools have proved their efficiency in surface treatments [for cleaning purposes (Ref 10), topography modification (Ref 11), heat treatment (Ref 12), etc.]. Laser surface treatment offers several advantages such as easy automation, localized treatment area, three-dimensional treatment, and great flexibility. A controlled interaction between the laser and material enables surface modification processes for all

Robin Kromer, Université de Bourgogne Franche Comté, UTBM IRTES-LERMPS, Belfort Cedex 90010, France; **Sophie Costil**, IRTES-LERMPS Institute, UTBM, Belfort Cedex 90010, France; **Jonathan Cormier**, Institut Pprime, Mechanics and Materials Science Laboratory, UPR CNRS 3346, ISAE-ENSMA, Téléport 2, 1, Avenue Clément Ader, BP 40109 86961 Chasseneuil-Futuroscope, France; and **Laurent Berthe**, **Patrice Peyre**, and **Damien Courapied**, PIMM, UMR 8006 CNRS, Arts et Métiers Paristech, 151 Bd De l'Hôpital, 75013 Paris, France. Contact e-mail: robin.kromer@gmail.com.

types of materials such as glasses, ceramics, polymers, and metals (Ref 13). A specific laser tool adapted (in terms of wavelength, pulse duration, spot size, and pulse frequency) to the material to be treated, combined with a scanner for three-dimensional shape modification, could promote mechanical and physicochemical bond strength for thick coatings elaborated by thermal spraying. Laser processing parameters have been shown to influence not only the surface topography but also the microstructure of the material due to the heat flux absorbed during such treatment (Ref 14, 15). The interaction between the laser and material is typically described by considering three main factors: the laser light, the material, and the environment. Conversion of the absorbed energy into heat via collisions is the most important effect. The energy supplied is sufficient for ablation (fast transition from overheated liquid to a mixture of vapor and drops) of micrometric layers (Ref 16). Using a scanner or automated microstepping stage, specific patterns can be produced on a surface according to the product application(s). Furthermore, laser patterning

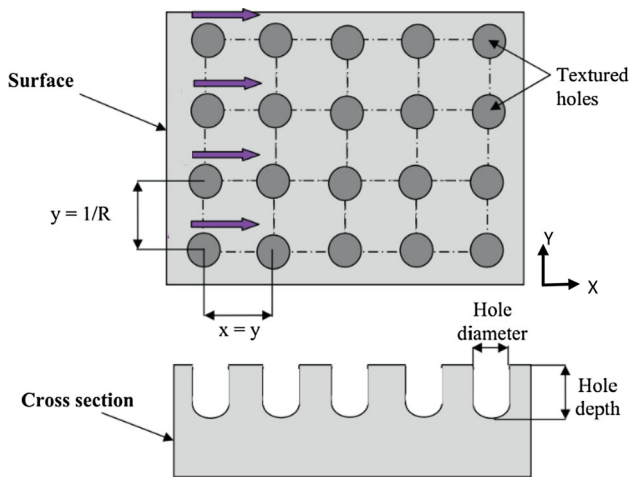


Fig. 1 Shallow spot-shaped cavities

can offer a solution to remove bond coats in different cases (e.g., thermal barrier coating systems) based on the interlocking effect in the substrate–coating couple.

In this study, a comparison between a conventional surface treatment method (grit blasting) and laser surface patterning was carried out to identify which main surface topography parameters are involved in the tensile and shear stresses. The results are presented and characterized based on standard adhesion methods to determine the interface toughness with different mechanical and physicochemical forces for two coating–substrate couples (Ref 17).

2. Experimental Procedures

2.1 Materials

As initial materials for study, 2017 aluminum alloy substrates (Mg=0.6 %, Cu=4 %, Mn=0.7 %, Fe=0.7 %, and Si=0.5 %; wt.%) were used (solution heat-treated). The substrates were buttons with thickness of 10 mm and diameter of 25 mm. The aluminum alloy chosen for this study is widely used in aircraft structural applications. Embrittlement problems occur during conventional surface pretreatment of ductile material such as 2017 Al alloy (Ref 9). The powder deposited on the substrates was NiAl (95 to 5 wt.%, AMDRY 956, Sulzer-Metco) with particle size from 45 to 90 μm ($d_{0.1}$ to $d_{0.9}$) with mean of 67 μm .

For the second couple, AISI 304L stainless steel substrates (C=0.07 %, Si=1 %, Mn=2 %, P=0.045 %, S=0.015 %, Cr=18 % Ni=9 %; wt.%) were selected. The substrates were buttons with thickness of 10 mm and diameter of 25 mm. Its properties (Young's modulus 193 MPa, toughness 175HV, thermal conductivity 16.2 W/m-K) make it an ideal candidate to replace the nickel-based superalloy (AM1) used in aeronautic engine turbine blades at room temperature, although not at the expected in-service AM1 temperatures on the order of 950 to 1100 °C (differing properties and oxidation) (Ref 18). The

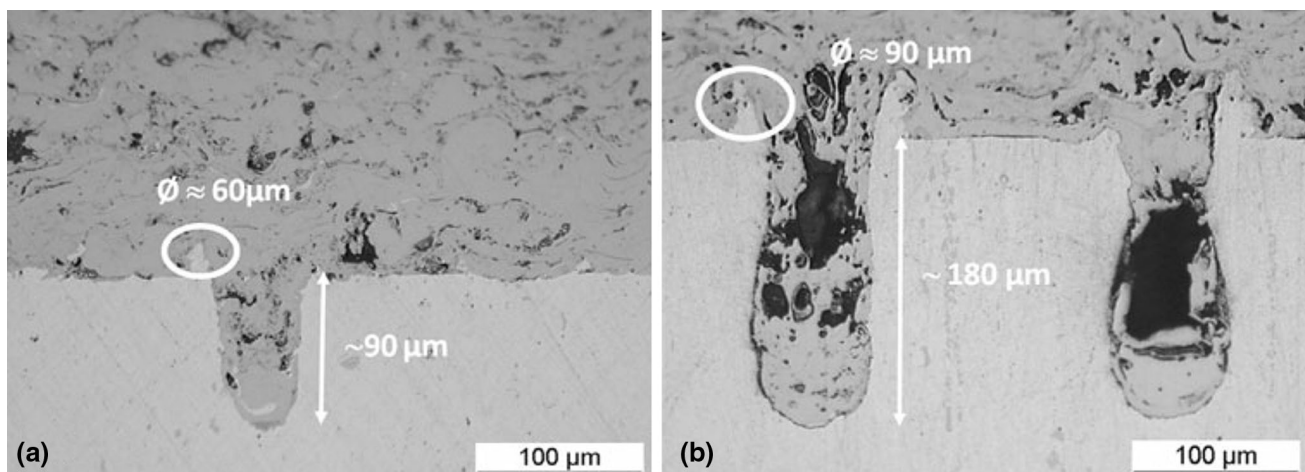


Fig. 2 Optical cross-sectional micrographs of AMDRY 956 (Ni5Al) powder plasma-sprayed onto aluminum AISI 2017 textured under different conditions (Ref 19): (a) 10 W, 40 kHz, 32 pulses and (b) 17.3 W, 20 kHz, 48 pulses

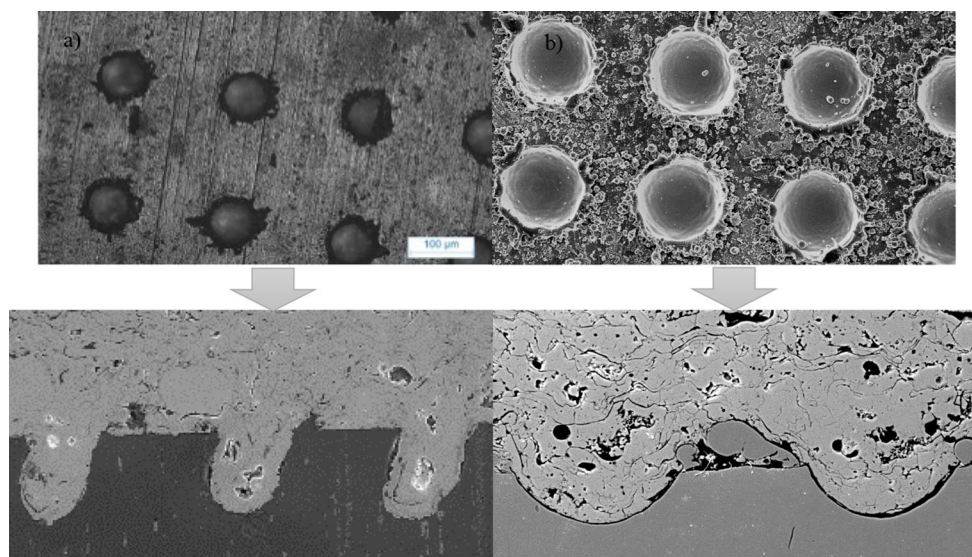


Fig. 3 Example top view and cross-sections for (a) 2017 Al surface patterning (F200) and (b) AISI 304L surface patterning (S80-150)

substrates were coated with a thermal barrier coating of $\text{ZrO}_2\text{-7Y}_2\text{O}_3\text{-1.7HfO}_2$ powder (Praxair-ZRO 236-1) with particle size from 16 to 100 μm ($d_{0.1}$ to $d_{0.9}$) with mean of 63 μm . Thermal barrier coatings (TBCs) are highly advanced materials that are usually applied to protect turbine blades from high temperature (Ref 19).

2.2 Substrate Pretreatment

For substrate pretreatment, several processes were carried out. Grit blasting (GB) was performed using an Econoline machine. Samples were treated with tangent 3 bar pressure at 5 cm to obtain roughness of $R_a \approx 6.7$ and $R_z \approx 33$ μm for 2017 aluminum alloy and $R_a \approx 4.5$ μm and $R_z \approx 28.3$ μm for AISI 304L stainless steel.

For laser treatment, experiments were conducted using a pulsed fiber laser (Laseo, Ylia M20, Quantel France). The laser operates at nominal wavelength of 1.06 μm with pulse duration of 100 ns, maximum power of 20 W, and variable frequency between 10 and 100 kHz. The laser beam is circular with diameter of 60 μm at the focal point and Gaussian energy distribution. The laser patterning consisted of a series of equidistant lines covered with a number of holes (to form a spotted surface). The scanner stops the laser beam, and pulses are generated to form the holes. Several shapes can be defined for different X - Y scans and number of pulses (Fig. 1). The topography changed strongly. The optimal pattern dimensions were studied depending on the spray process (sprayed powder and melted particle viscosity). As shown in Fig. 2, deep and wide holes affected the adhesion bond strength since the coating did not provide good contact (Ref 20).

In this study, a hole pattern was chosen. Thus, the textured substrate has an adhesion area that depends on the shape, height, orientation, distribution, and density of holes. A hole volume equal to the particle volume and a hole opening larger than the particle diameter were applied as criteria.

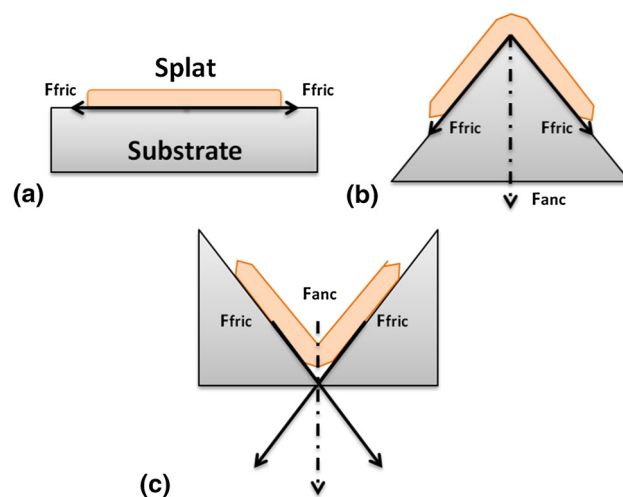


Fig. 4 Sketch of the anchoring force (F_{Anc}) of a splat as a function of the in-contact surface shape

For 2017 aluminum alloy, the holes followed four grid patterns. Holes were formed with diameter of 60 μm and depth of 80 μm (F[L]), where [L] refers to the distance between two holes in μm along the X and Y directions (100, 150, 200, and 300 μm).

For AISI 304L stainless steel, large particle size was used. Two hole patterns (S{D}-[L]) were formed with diameter {D} of 60 and 80 μm and depth of 35 and 40 μm . Figure 3 shows an example of the textured surface for 2017 Al and AISI 304L (top view and cross-section).

2.3 Morphological Analyses

Characterization of the morphology of pretreated samples with and without coating was performed by optical microscopy (MOZ2 Zeiss) and scanning electron

microscopy (SEM, JEOL JSM 6400). The in-contact area was computed using image analysis to compare the adhesive bond strength between the different surface treatments.

Melted particles recede on the surface during thermal spray, causing the coating to become trapped on the surface after solidification. Quenching stresses and/or residual stresses are created. The interface mechanical force is dependent on the stresses, friction forces, and blocking mechanisms (Fig. 4). If a thin object (splat) is placed on an inclined plane (Fig. 5), a pressure P is applied. The friction force f is characterized as

$$f = \mu Ps, \quad (\text{Eq 1})$$

where μ and s are the friction coefficient and contact area, respectively. f_v is the force needed to remove the object vertically, i.e.,

$$f_v = f \cos \theta. \quad (\text{Eq 2})$$

This removal force f_v is proportional to the projected area. The surface roughness can be expressed using the following function in orthogonal coordinates:

$$z = f(x, y). \quad (\text{Eq 3})$$

If a thermally sprayed coating fills the surface, the vertical force df_v required to remove the coating from an infinitesimal area ds can be expressed as

$$df_v = \mu P ds \cos \theta, \quad (\text{Eq 4})$$

where θ is the angle between the vertical and the infinitesimal region. The total force for a domain D is therefore

$$\int_D df_v = \int_S \mu P \cos \theta ds = \bar{\mu} \bar{P} \int_S \cos \theta ds, \quad (\text{Eq 5})$$

where μ and P are replaced by their mean. Consequently, the adhesive bond strength is

$$F = \frac{\bar{\mu} \bar{P} \int_S \cos \theta ds}{D}. \quad (\text{Eq 6})$$

F can be computed theoretically from R (the in-contact ratio, computed by image analysis) as

$$F = \bar{\mu} \bar{P} R. \quad (\text{Eq 7})$$

Therefore, R can be used as a criterion for the mechanical adhesion force. The in-contact ratio R represents the ratio in contact between the coating and substrate per unit surface area (Eq 8). The surface ratio R was determined by image analysis (Fig. 6, 7). The interface was analyzed and the length computed using ImageJ software and algorithms (Fig. 6).

$$R = \frac{\text{Adhesion area}}{\text{Plane area}}. \quad (\text{Eq 8})$$

Patterns add 6 to 10 times the in-contact surface. Table 1 presents the surface area ratio for the grit blasting and laser treatments. The in-contact ratio strongly depends on the grid pattern. Large values are obtained for laser patterning compared with grit blasting.

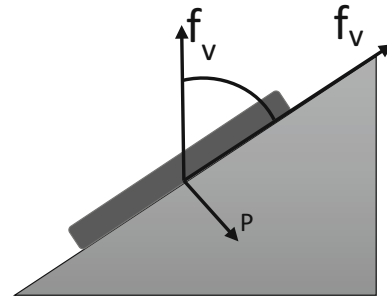


Fig. 5 Illustration of the mechanical friction force on the interface between a thin object and an inclined plane

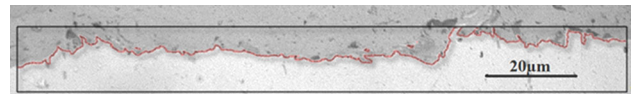


Fig. 6 Image analysis of adhesion area: grit-blasted surface with the computed interface in red (Color figure online)

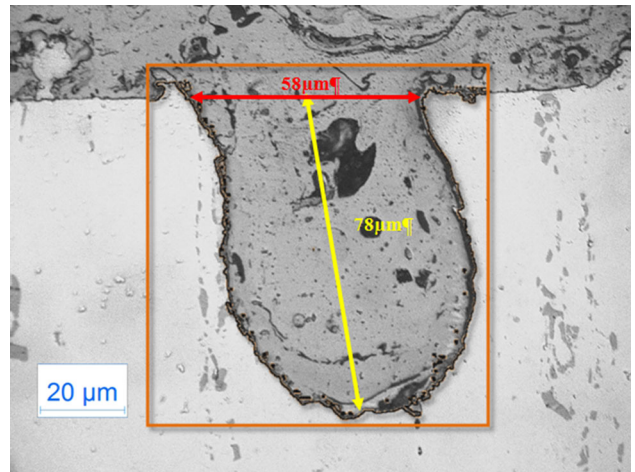


Fig. 7 Image analysis of surface area for laser surface texturing, with the interface computed for one keyhole in red (each keyhole adds 11 times the adhesion area compared with a planar surface) (Color figure online)

Table 1 Surface area ratios for grit blasting (GB) with 100, 150, 200, and 300 grids for different patterns

Holes	Grid [L]				GB
	100	150	200	300	
F[L]	7.3	3.7	2.5	1.7	2.7
S60-[L]	6.4	3.1	2.1	1.3	1.8
S80-[L]	6.9	3.4	2.3	1.4	

2.4 Coating Production

NiAl and YSZ coatings were deposited using standard thermal spray parameters (Ref 21, 22) (Table 2). Thick

coatings (300 μm) were produced by atmospheric plasma spraying with an F4 torch (Sulzer-Metco, Neuwiesenstrasse 158401, Winterthur, Switzerland) mounted on an XYZ robot (ABB robot, Affolternstrasse 44, CH-8050 Zurich, Switzerland). The samples were moved rotationally and the torch moved vertically for homogeneous coating deposition. Samples were cooled down to room temperature using a perpendicularly guided air jet.

2.5 Adhesion Tests

Adherence tests were carried out to provide values for each system. A simple unidirectional test will result in different stresses locally (multiscale effect) (Fig. 8) (Ref 23).

Table 2 Thermal spray parameters defined for NiAl and YSZ powders

	NiAl		YSZ	
Primary gas flow rate, slpm	Ar	50	Ar	44
	H ₂	8	H ₂	13
Spray distance, mm		120		120
Arc current, A		600		630
Powder feed rate, g/mm		27		23
Carrier gas flow, L/min		3.3		3.4
Injection angle, °		75		90

The elastic body deforms and creates tensile and shear stresses near an interface (interfacial instabilities). Two adhesion tests were used to cover all stress possibilities.

Coating adhesion is usually tested by pull-off tests (described in DIN EN 582-ASTM standard C633). The tested

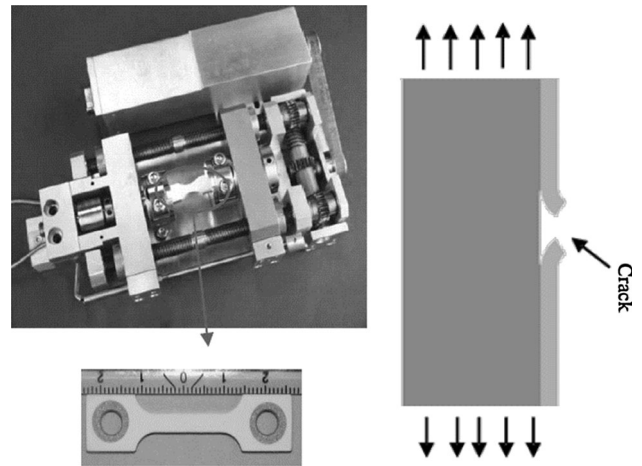


Fig. 9 Microtensile stage, global view of the system; coated specimen; schematic view of coating failure with crack propagating through the coating then to the interface

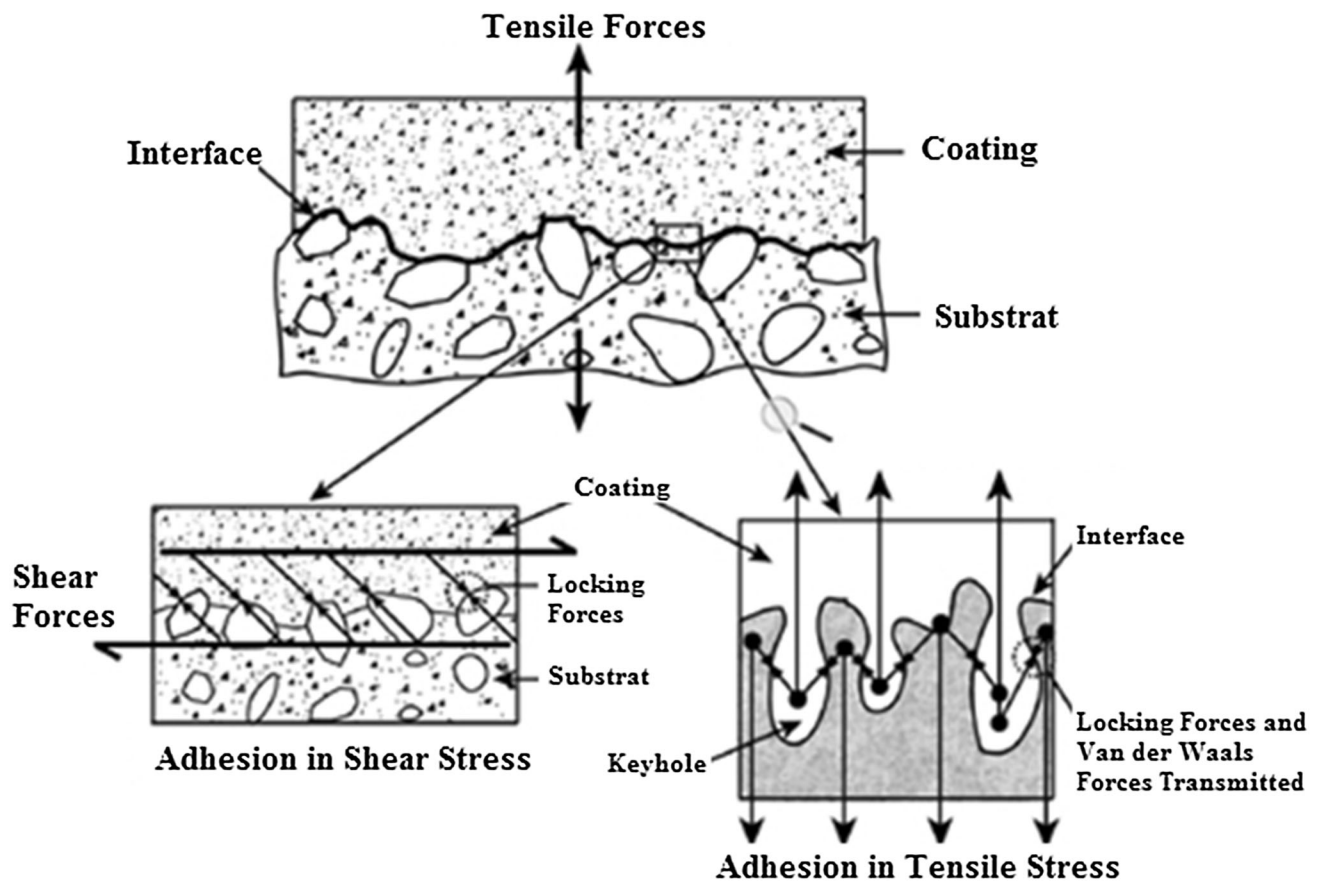


Fig. 8 Adhesion in tensile and shear stress

samples were buttons joined with cylindrical counterparts using adhesive film (FM1000). A constant displacement rate (1.026 mm/s) was applied using a tensile test machine to complete failure. The maximum force was attributed to the adherence at the interface for the considered surface.

Secondly, another testing procedure was used to characterize the adhesion under shear mode, namely in-plane tensile tests using a tensile microstepped stage (DEBEN micromachine) under a light microscope. The sample geometry was defined according to the standard tests of ISO 6892 (Fig. 9). Top-view pictures of the specimen surface were captured during tensile testing with the coating located on the edges. NiAl-Al2017 samples were used. The displacement rate was 10 $\mu\text{m/s}$. When the crack had propagated through the coating, the energy was released through the interface and the test stops.

3. Results

Tensile adhesion tests were performed on the previously described coating–substrate samples to evaluate the interface energy for the surface preparations. Figure 10 shows the adherence values for the NiAl–Al2017 couple. The cohesive bond strength of the coating was estimated to be 60 MPa. The grit-blasted surface (GB) gives an expected adhesive failure (Ref 24), i.e., adhesive debonding, at about

25 MPa. The laser-treated substrates (F150, F200, and F300 grids) failed at the interface at larger values (52, 35, and 34 MPa, respectively). An unexpected cohesive failure occurred in the samples treated with the closest holes (F100).

Figure 11 shows the pull-off test results for the YSZ–AISI 304L couples. Similar behavior was observed. The adhesion strength was 11 MPa for the grit-blasted surface. The adhesive bond strength was 4, 7, 14, and 30 MPa for the 300, 200, 150, and 100 μm grid, respectively, for the S60 patterns and 5, 10, 19, and 33 MPa for the S80 patterns. Cohesive failure occurred for the closest holes and largest holes (S80-100).

Figure 12 shows cross-sections of tested specimens with adhesive and cohesive failure. According to these cross-sections, different fracture modes can be noted for the grit-blasted and laser-treated surfaces. The patterned surfaces show mixed-mode (adhesive and cohesive) failure. Few particles are locked at the interface after grit blasting (Fig. 12a–d) compared with laser patterning. The coating is locked in the holes, which hence act as anchors (Fig. 12b–e). Cohesive failure is observed for the closest configuration (Fig. 12c–f). The interface bond strength was higher than the coating cohesive bond strength. Cracks stopped near holes (obstacles), increasing the interface energy release rate.

The stress during pull-off tests is mainly tensile, hence another test was carried out, viz. in-plane testing (with mainly shear stress), on both grit-blasted and laser-treated surfaces (F200 and F100). Four specimens were tested.

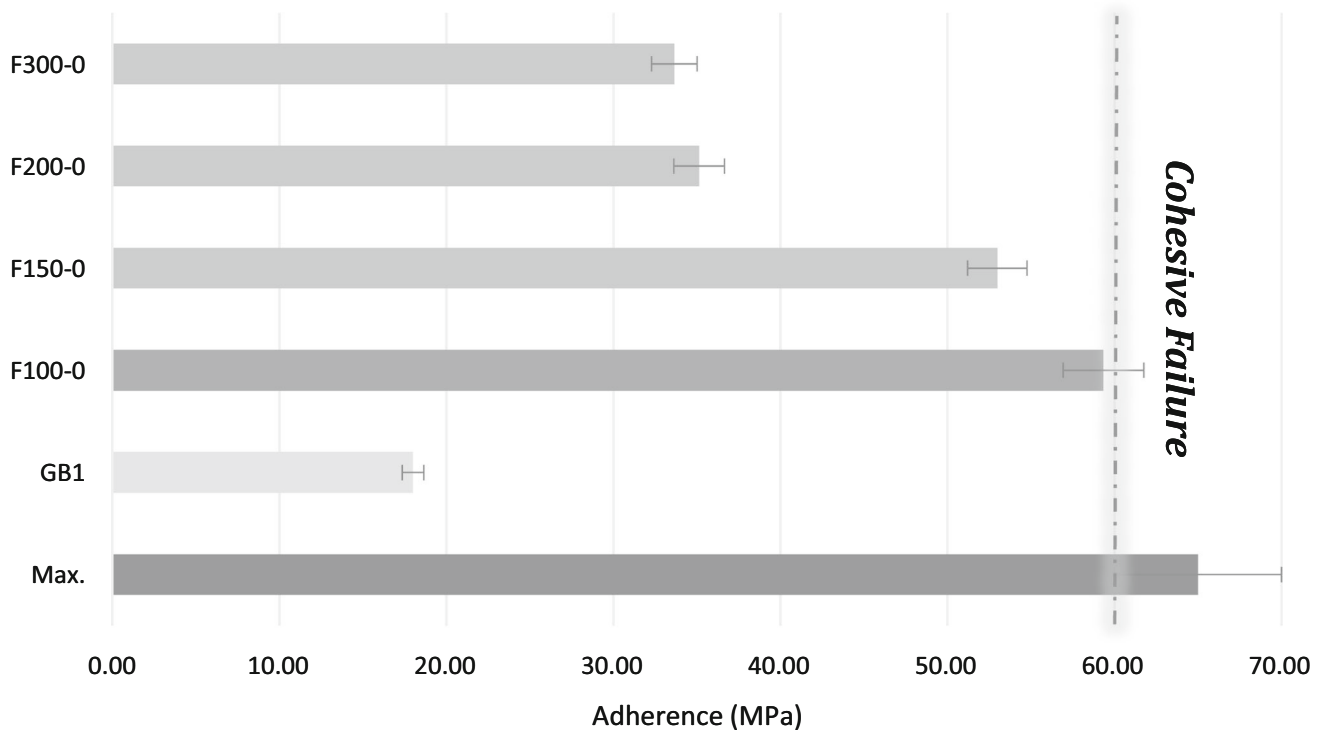


Fig. 10 Results of tensile adhesion tests for NiAl coating elaborated on grit-blasted and different patterned 2017 aluminum alloy substrate

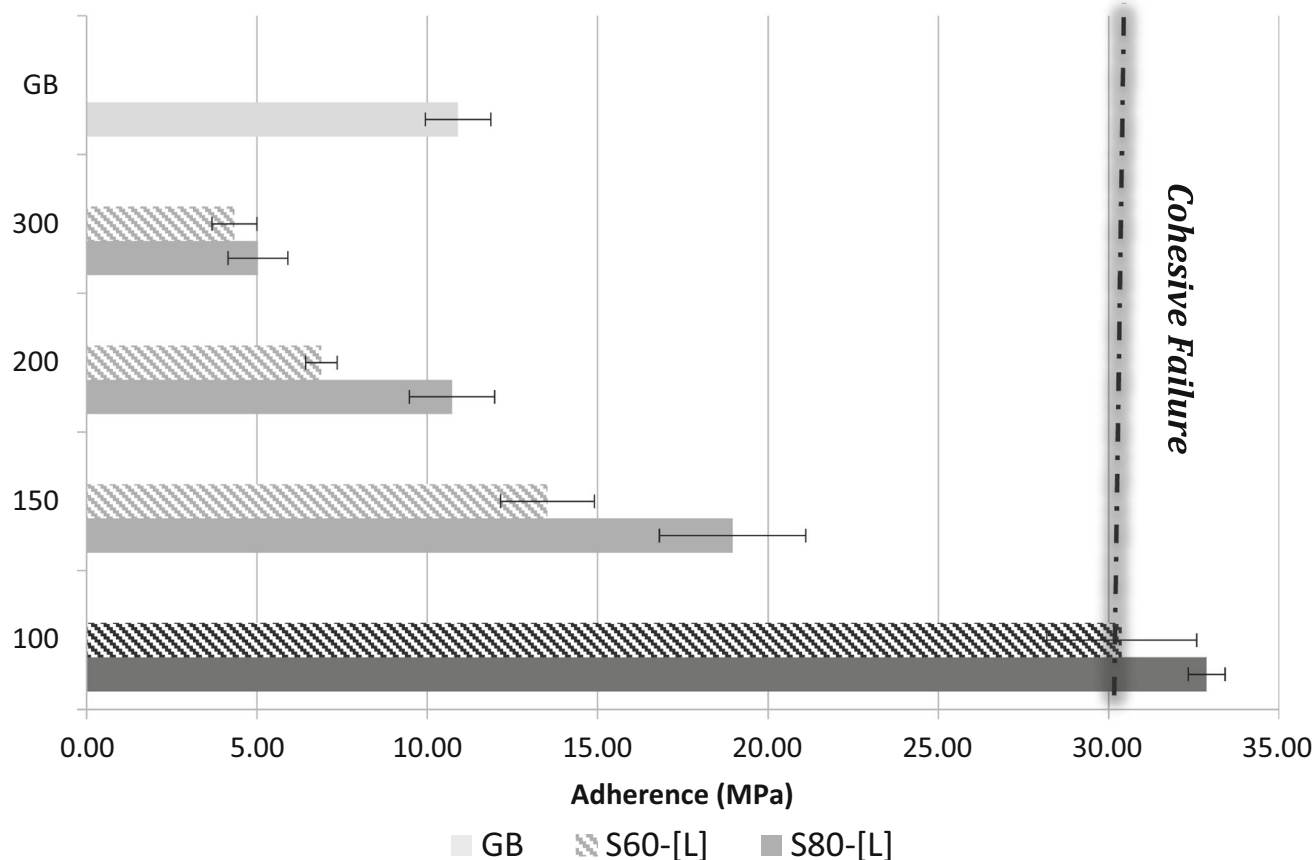


Fig. 11 Results of tensile adhesion tests for YSZ coating sprayed on grit-blasted and different patterned AISI 304L stainless steel substrates

Cracks of 1344 ± 345 , 234 ± 34 , and 148 ± 22 μm were identified, respectively (with the crack going through the coating and through the interface due to the energy released). Different behaviors occurred according to the interface morphology (Fig. 13). Cracks followed the interface, but the coating was also trapped in holes (going around or through). The obstacles diminished the energy released at the interface due to the mixed-mode failure.

4. Discussion

Firstly, the pattern shape and sprayed particles must be adapted for good contact (to be detailed in a future paper). The adopted hole shape seems to be correct (with good filling, as illustrated in Fig. 12). The porosity ratio is larger in the holes than for the coating, but the difference is negligible.

A comparison between the standard and innovative surface preparation methods is illustrated in Fig. 14 (by the adherence values for different in-contact ratios R). The laser-treated surface slope is twice that for the grit-blasted surface (NiAl–Al2017: 15.75 for LST and 8.18 for GB; YSZ–AISI 304L: 7.47 for LST and 4.53 for GB). The

adhesive bond strength is doubled for the same contact area. On the one hand, R cannot be larger than 3.5 for the grit-blasted surface. On the other hand, the adhesive bond strength has a limit for the laser-treated surface (with cohesive toughness of 34 MPa). Therefore, the adhesive bond strength can be calculated analytically for both treated surfaces. The grit-blasting limits are about 25 and 18 MPa, while those for laser surface texturing are about 112 and 44 MPa, for couple 1 and 2, respectively.

Many important interface fracture problems involve mixed-mode (shear and opening) displacement along crack surfaces following linear elastic fracture mechanics (LEFM). Interface fracture must be influenced by non-planarity of the interface and by the phase angle of loading. The adhesion energy as a function of the phase angle of loading has been determined by Hutchinson et al. (Ref 25) to be

$$G_i = G_{II}(1 + \tan^2(\psi(1 - \lambda))), \quad (\text{Eq 9})$$

where λ is a material parameter corresponding to the interface, ψ is the phase angle of loading, and G_{II} is the energy release rate in mode I. A limit for the energy release rate to kink out in the coating (crack propagating through coating) can be calculated. Cracks can propagate

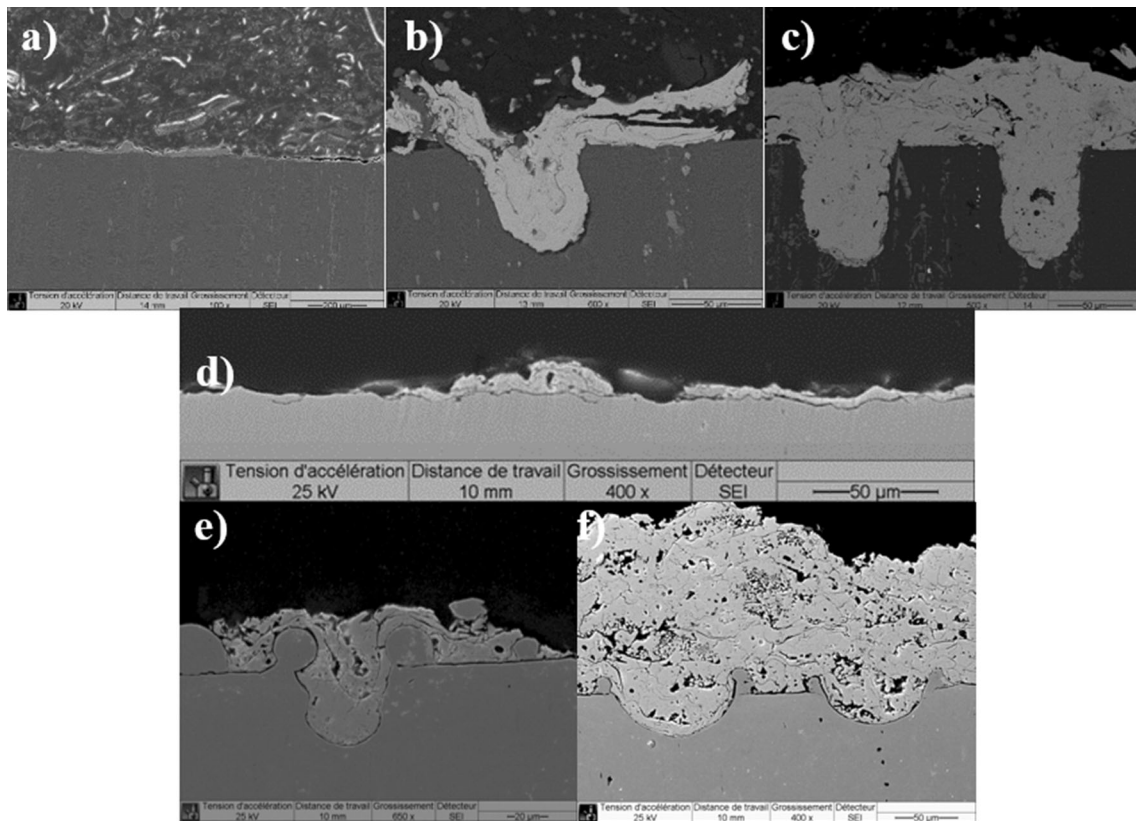


Fig. 12 Micrographs presenting the interface after tensile testing for (a) grit-blasted surface, (b) F200-30, and (c) F100-0 for NiAl-AI2017 and (d) grit-blasted surface, (e) S60-150, and (f) S80-100 for YSZ-AISI 304L

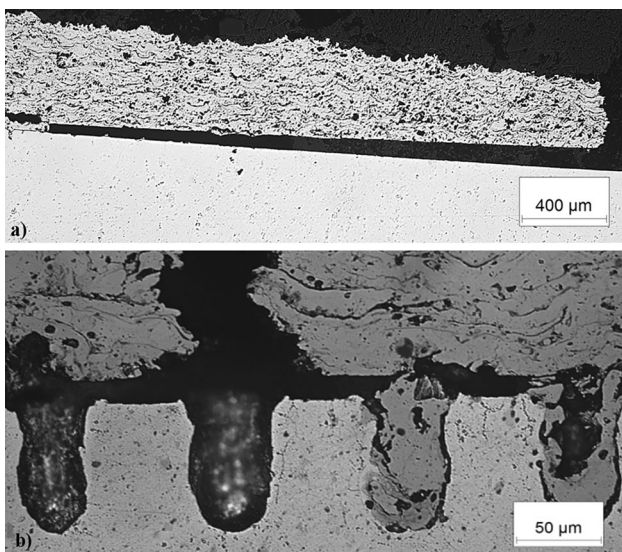


Fig. 13 Microscopic observations of crack propagation during in-plane testing of NiAl-AI2017 for (a) grit-blasted and (b) laser-treated samples

easily on planar surfaces, so holes are considered isolated. Cracks are stopped in front of and/or go around each hole. Cracks are deflected in the coating due to the sharp edges.

Straight crack propagation (going through the coating) between intersplat interfaces is easier than following the interface, because of the altered phase angle near holes. The macroscopic interfacial toughness depends on the interface energy and mechanical anchoring. The total adhesive bond strength for a textured surface can be considered to be the superposition of the adhesive and cohesive strength.

Therefore, the cohesive zone ratio was calculated as a function of the patterning (Fig. 15). The assumption is cohesive failure above each hole (cohesive zone = hole diameter) and adhesive failure on the plateau. Figure 16 shows the adherence as a function of the cohesive zone ratio for both couples. The number of holes per unit surface area increases for the different grid patterns, and the adhesive bond strength changes linearly. Firstly, for the plane surface (cohesive zone ratio = 0), the adherence values are 12 and 0 MPa for NiAl-AI2017 and YSZ-AISI 304L, respectively, corresponding to physical bonding. Then, the coating cohesive energy release rate is represented by the slope. The cohesive energy release rate is larger for the NiAl than the YSZ coating. Consequently, mixed-mode failure has a stronger effect.

Numerical analysis of crack propagation for different stresses will be developed in the future, enabling computation of the optimal pattern morphology for use and choice of material couples. After validation, the presented

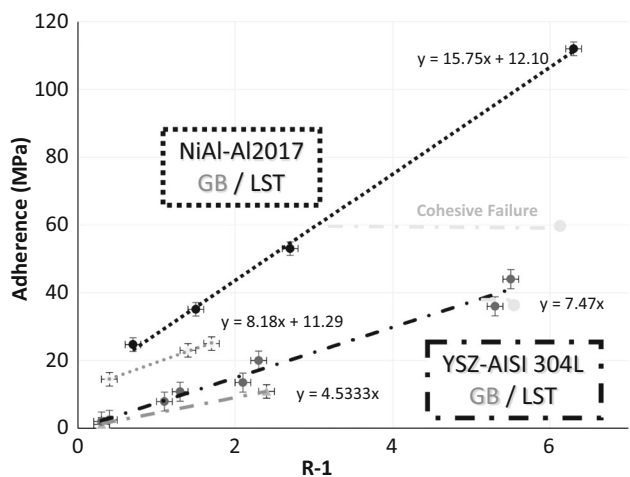


Fig. 14 Adherence as a function of R for NiAl-AI2017 and YSZ-304L couples

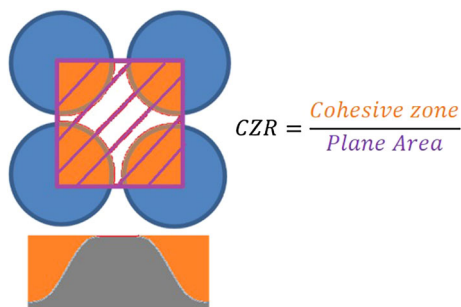


Fig. 15 Cohesive zone ratio computation

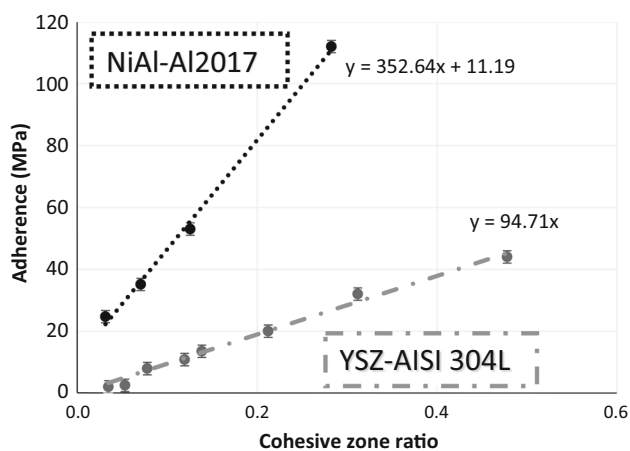


Fig. 16 Adherence as a function of cohesive zone ratio for NiAl-AI2017 and YSZ-304L couples for LST

method can be used as a guideline in the thermal spray industry to improve interface adhesion; For example, based on initial results, bond coat removal for thermal barrier application is possible due to the large adhesive bond strength.

5. Conclusions

Application of laser micropatterning of a substrate surface to increase coating adhesion has been studied. The textured surface with optimized hole morphology enables interesting adhesion values to be obtained, being higher than those generally observed after conventional pretreatment. The adhesive bond strength was multiplied by two for both coating-substrate couples (metallic-metallic and ceramic-metallic) for similar contact area. Holes indeed create obstacles to interfacial crack propagation. Cracks go through the coating, increasing the energy required (due to mixed-mode failure). The interface bond strength is larger than the cohesive toughness for the closest holes. The periodicity of the pattern has an effect on the adherence due to mechanical anchoring, which stops crack propagation for different applied stresses.

Secondly, the influence of the substrate surface topography was studied and its effects on coating adhesion determined. The adhesive bond strength is linearly proportional to the contact area. The macroscopic bond strength is linearly dependent on the cohesive zone. Prediction of the adhesive bond strength is possible based on the pattern morphology and periodicity. The effectiveness of laser surface patterning for surface treatment to enhance the adhesive bond strength has been demonstrated, with mixed-mode failure being a key issue.

Acknowledgments

The authors gratefully acknowledge the ANR for financial assistance through the ARCOLE (12-BS09-0009) project. A part of this study was conducted in the framework of the LABEX INTERACTIFS at Institut Pprime UPR CNRS 3346 under contract number ANR-11-LABX-0017. F. Hamon and C. Adam are gratefully acknowledged for their expertise in SEM and thermal spray processes for analysis and coating deposition optimization.

Open Access

This article is distributed under the terms of the Creative Commons Attribution 4.0 International License (<http://creativecommons.org/licenses/by/4.0/>), which permits unrestricted use, distribution, and reproduction in any medium, provided you give appropriate credit to the original author(s) and the source, provide a link to the Creative Commons license, and indicate if changes were made.

References

1. M. Boulos, P. Fauchais, and E. Pfender, *Thermal Plasma Fundamentals and Application*, Vol 1, Plenum, New York, 1994
2. S. Chandra and P. Fauchais, Formation of Solid Splats During Thermal Spray Deposition, *J. Therm. Spray Technol.*, 2009, **18**(2), p 148-180

3. M. Fukumoto, T. Yamaguchi, M. Yamada, and T. Yasui, Splash Splat to Disk Splat Transition Behavior in Plasma-Sprayed Metallic Materials, *J. Therm. Spray Technol.*, 2007, **16**(5–6), p 905-912
4. J. Cedelle, M. Vardelle, and P. Fauchais, Influence of Stainless Steel Substrate Preheating on Surface Topography and on Millimeter- and Micrometer-Sized Splat Formation, *Surf. Coat. Technol.*, 2006, **201**(3–4), p 1373-1382
5. R.N. Wenzel, Resistance of Solid Surfaces to Wetting by Water, *Ind. Eng. Chem.*, 1936, **28**(8), p 988-994
6. K. Yang, M. Fukumoto, T. Yasui, and M. Yamada, Role of Substrate Temperature on Microstructure Formation in Plasma-Sprayed Splats, *Surf. Coat. Technol.*, 2013, **214**, p 138-143
7. F. Bahbou, P. Nylen, and S. Trollhattan, Relationship Between Surface Topography Parameters and Adhesion Strength for PS, *ITSC 2005*, 2005
8. Y. Feng, Z. Liu, R. Vilar, and X.-S. Yi, Laser Surface Cleaning of Organic Contaminants, *Appl. Surf. Sci.*, 1999, **150**(1), p 131-136
9. L. Sluatinianu, S. Potarniche, M. Coteata, I. Grigoras, L. Gherman, and F. Negoescu, Surface Roughness at Aluminium Parts Sand Blasting, *Proc. Manuf. Syst.*, vol. 6, no. 2, 2011
10. C. Coddet, G. Montavon, S. Ayrault-Costil, O. Freneaux, F. Rigolet, G. Barbezat, F. Folio, A. Diard, and P. Wazen, Surface Preparation and Thermal Spray in a Single Step: The PROTAL Process—Example of Application for an Aluminum-Base Substrate, *J. Therm. Spray Technol.*, 1999, **8**(2), p 235-242
11. A. Kovalchenko, O. Ajayi, A. Erdemir, G. Fenske, and I. Etsion, The Effect of Laser Surface Texturing on Transitions in Lubrication Regimes During Unidirectional Sliding Contact, *Tribol. Int.*, 2005, **38**(3), p 219-225
12. Y. Danlos, S. Costil, H. Liao, and C. Coddet, Combining Effects of Ablation Laser and Laser Preheating on Metallic Substrates before Thermal Spraying, *Surf. Coat. Technol.*, 2008, **202**(18), p 4531-4537
13. I. Etsion, State of the Art in Laser Surface Texturing, *J. Tribol.*, 2005, **127**(1), p 248
14. M. Medale, C. Xhaard, and R. Fabbro, A Thermo-Hydraulic Numerical Model to Study Spot Laser Welding, *Comptes Rendus Mécanique*, 2007, **335**(5–6), p 280-286
15. B.S. Schorr, K.J. Stein, and A.R. Marder, Characterization of Thermal Spray Coatings, *Mater. Charact.*, 1999, **42**(2), p 93-100
16. D. Marla, U.V. Bhandarkar, and S.S. Joshi, Modeling Nanosecond Pulsed Laser Ablation: A Focus on Temperature Dependence of Material Properties, *Manuf. Lett.*, 2014, **2**(2), p 13-16
17. R. Kromer, S. Costil, J. Cormier, D. Courapied, L. Berthe, P. Peyre, and M. Boustie, Laser Surface Patterning to Enhance Adhesion of Plasma Sprayed Coatings, *Surf. Coat. Technol.*, 2015, **278**, p 171-182
18. F. Raillant, J. Cormier, A. Longuer, X. Milhet, and J. Mendez, High-Temperature Creep Degradation of the AM1/NiAlPt/EBPVD YSZ System, *Metall. Mater. Trans. A*, 2014, **45A**, p 351-359
19. D.R. Clarke and S.R. Phillpot, Thermal Barrier Coating Materials, *Mater. Today*, 2005, **8**(6), p 22-29
20. D. Garcia-Alonso, N. Serres, C. Demian, S. Costil, C. Langlade, and C. Coddet, Pre-/During-/Post-Laser Processes to Enhance the Adhesion and Mechanical Properties of Thermal-Sprayed Coatings with a Reduced Environmental Impact, *J. Therm. Spray Technol.*, 2011, **20**(4), p 719-735
21. S. Costil, H. Liao, A. Gammoudi, and C. Coddet, Influence of Surface Laser Cleaning Combined with Substrate Preheating on the Splat Morphology, *J. Therm. Spray Technol.*, 2005, **14**(1), p 31-38
22. Y. Chen, Y. Tan, S. Tessarini, and S. Sampath, Integrated Study of APS YSZ Coatings with Different Spray Angle, *J. Therm. Spray Technol.*, 2013, **22**(2–3), p 110-115
23. C.C. Berndt, Tensile Adhesion Testing Methodology for Thermally Sprayed Coatings, *J. Mater. Eng.*, 1990, **12**, p 151-158
24. M.S. Morsi, S.A.A. El Gwad, M.A. Shoeib, and K.F. Ahmed, Effect of Air Plasma Sprays Parameters on Coating Performance in Zirconia-Based Thermal Barrier Coatings, *Int. J. Electrochem. Sci.*, 2012, **7**, p 2811-2831
25. J.W. Hutchinson and Z. Suo, Mixed Mode Cracking in Layered Materials, *Adv. Appl. Mech.*, 1992, **29**, p 64-163